Carbon 167 (2020) 646–657

Contents lists available at ScienceDirect

Carbon

journal homepage: www.elsevier.com/locate/carbon

Nitrene functionalization as a new approach for reducing the interfacial thermal resistance in graphene nanoplatelets/epoxy nanocomposites

Sebastien Depaifve [a, b], Carlos Eloy Federico [a], David Ruch [a], Sophie Hermans [c], Abdelghani Laachachi [a, *]

[a] Department of Materials Research and Technology (MRT), Luxembourg Institute of Science and Technology (LIST), ZAE Robert Steichen, 5 Rue Bommel, 4940, Hautcharage, Luxembourg
[b] Université du Luxembourg, 2 avenue de l'Université, 4365, Esch-sur-Alzette, Luxembourg
[c] IMCN Institute, Université catholique de Louvain, 1 Place L. Pasteur, 1348, Louvain-la-Neuve, Belgium

ARTICLE INFO

Article history:
Received 4 March 2020
Received in revised form
28 May 2020
Accepted 11 June 2020
Available online 20 June 2020

ABSTRACT

Conventional functionalization methods, such as oxidation, can be very damaging for the nanocarbons microstructure and therefore detrimental for their intrinsic thermal conductivity. In this study, nitrene chemistry was investigated as a non-disruptive approach for the covalent functionalization of graphene nanoplatelets (GNP). The nitrene precursor was synthesized and thermally decomposed *in situ* to functionalize GNP (cm-GNP). Temperature and solvents of reaction were found to have profound impact on the functionalization yield. Epoxy nanocomposites were then prepared with pristine, oxidized and cm-GNP. Influence of dispersion methodology was crucial for cm-GNP, as sonication was found to damage the functionalization. Oxidation caused a dramatic drop in thermal conductivity compared to pristine GNP. By contrast, nitrene chemistry produced the highest thermal conductivity enhancement. Finally, epoxy nanocomposites thermal conductivity results were correlated and discussed in light of SEM and micro-computed X-ray tomography (μCT) analyses. The μCT highlighted new features, such as micro-voids surrounding pristine GNP in epoxy nanocomposites, which are invisible with conventional methods. It was found that functionalization not only enhanced the dispersion but also improved GNP/polymer interactions. Moreover, μCT clearly demonstrated that nitrene functionalization eliminated the micro voids surrounding the fillers in the epoxy nanocomposites.

1. Introduction

Thermal dissipation has become a major issue in many technical fields such as electronics, LED lightings, batteries, etc. [1,2]. Efficient thermal management is crucial to maintain a safe working temperature and improve the lifespan of the device [3]. Heat dissipation is usually achieved using highly thermally conductive metallic materials. However, many modern applications would benefit from polymeric materials because of their shapeability, flexibility, lightweight and low-cost [4]. Unfortunately, bulk polymer materials exhibit a low intrinsic thermal conductivity (~0.1–0.5 W/mK) [5]. Consequently, researchers started developing highly thermally conductive polymer composites.

Since their discovery, carbon fillers such as carbon nanotubes (CNT), expanded graphite (EG) and graphene nanoplatelets (GNP) have attracted a lot of interest in polymer composites due to their exceptional thermal, gas barrier, chemical resistance and electrical properties [6]. Balandin et al. [7] measured the outstanding thermal conductivity of graphene (~4.800–5.500 W/mK) based on Raman spectroscopy and paved the way towards new high thermally conductive polymer composites materials.

However, extensive research over the past decade has shown that the exceptional thermal conductivity of carbon fillers does not produce polymer composites with extremely high thermal conductivity [8]. The thermal performances of nanocarbon/polymer composites are still underperforming due to poor interactions between the fillers and the polymer matrix. It has been shown that poor interaction leads to a dramatic interfacial thermal resistance,

* Corresponding author.
E-mail address: abdelghani.laachachi@list.lu (A. Laachachi).

https://doi.org/10.1016/j.carbon.2020.06.035
0008-6223/

sometimes referred as Kapitza resistance, between the fillers and the matrix [9]. The poor interaction is also responsible of the inhomogeneous dispersion of the fillers in nanocomposites [10,11].

Many theoretical works have suggested chemical functionalization of nanocarbons to reduce the interfacial thermal resistance and improve the compatibility of graphene/polymer nanocomposites [12–14]. The introduced chemical functions could act as a chemical and/or physical bridge to link the vibrational phonon spectra of the polymer to that of the nanocarbons [15]. Unfortunately, covalent modification of nanocarbons is complicated due to the high chemical stability of the sp^2 carbon lattice. Oxidation has been largely employed for the nanocarbons functionalization and proven to be efficient for their improved dispersion in various polymer matrixes [16–18]. However, oxidation requires harsh experimental conditions (concentrated oxidants and acids at elevated temperatures) and does not allow easy control of the functionalization chemistry on the graphene surface [19]. More importantly, oxidation introduces voids and defects in the graphene lattice, which can reduce dramatically the intrinsic thermal conductivity of the fillers [20–22].

Non-covalent approaches have been proposed theoretically and demonstrated experimentally for the compatibilization of carbons with polymers [15,23,24]. They have the benefit of not damaging the carbon lattice and therefore not affecting the intrinsic nanocarbon thermal conductivity. However, the non-covalent character of the interaction does not allow an efficient transfer of the molecular vibrations. Several theoretical papers have discussed the benefit of covalent modification compared to non-covalent approaches in order to improve the thermal transfer [14,25,26]. Unfortunately, these considerations are mainly based on theoretical work. Therefore, experimental confirmation is crucial to understand the effect of covalent modification on the thermal transfer in carbon/polymer nanocomposites.

In this paper, we investigate nitrene chemistry as a non-disruptive covalent functionalization approach for the surface modification of graphene nanoplatelets. This particular chemistry allows carbon atoms neighbouring the functionalization sites to be very little affected by the functionalization [27]. Therefore, nitrene chemistry is a promising approach to maintain a high intrinsic thermal conductivity in graphene, as the graphitic microstructure is mostly retained. In this work, we synthesized organic azide (azidopropanol) as nitrene precursor. We functionalized GNP via thermal decomposition of the as-synthesized organic azide. In parallel, we also prepared oxidized-GNP to compare the functionalization method's influence on the fillers thermal performances. The chemically modified GNP (cm-GNP) were characterized with TGA, SEM, XPS and Raman spectroscopy. Nanocarbon/epoxy composites were produced with pristine-GNP, cm-GNP and oxidized-GNP to assess the benefit of our approach. The thermal conductivity was measured and compared for the different composites. The thermal conductivity modulation is discussed with regards to the dispersion state of the fillers and interaction with the epoxy matrix via SEM and μCT analysis of the composites. We show that the functionalization not only helps improving the dispersion of the fillers but also allows increasing the thermal conductance and eliminating the micro-voids surrounding the nanocarbon fillers.

2. Experimental and instrumental methods

2.1. Materials

The graphene nano-platelets (GNP) used in this study were obtained from Strem chemicals (#06-0220) and have an average lateral size ~ 25 μm and an average thickness of ~6–8 nm. 3-chloro-1-propanol (98%) was supplied by Sigma-Aldrich and used as received. 1,2-dichlorobenzene (oDCB) 99% pure was purchased from Acros Organics and *N,N*-dimethylformamide (DMF) ≥ 99.5% pure was purchased from Carl Roth. The epoxy resin, D.E.R. 332, liquid epoxy resin based on bisphenol A diglycidyl ether (DGEBA) (manufactured by DOW chemicals) with 4,4′-diaminodiphenyl sulfone (DDS, 97%), as the hardener, were purchased from Sigma Aldrich. Both were used as received and their chemical structures are shown in Fig. 1.

2.2. Synthesis of 3-azido-1-propanol

In a typical synthesis, 3-chloro-1-propanol (4.727 g, 50 mmol, 1 eq.) was dissolved in 50 mL distilled water in a 100-mL round-bottomed flask equipped with a magnetic stirring bar. NaN_3 (4.55 g, 70 mmol, 1.4 eq.) was then added and the mixture was vigorously stirred under refluxing conditions for 24 h. The reaction mixture was then cooled down to room temperature. The product was extracted with 3 × 50 mL of Et_2O. The combined organic layers were dried over $MgSO_4$ while stirring. Finally, the product was filtered through a filter paper and concentrated in a rotary evaporator, to give a pale yellow oil. ^1H NMR and ^{13}C NMR spectra can be viewed in the S.I.

2.3. GNP functionalization

2.3.1. GNP modification using nitrene chemistry

In a typical experiment, GNP powder (600 mg, 50 mmol "carbon", 1 eq.) was mixed with 120 mL of oDCB or DMF in a 250-mL two-necked round-bottomed flask equipped with a magnetic stirring bar, a condenser and a rubber septum. The reaction vessel was purged with argon. The mixture was then heated up to 150 °C. Then, the synthesized 3-Azido-1-propanol (1.01 g, 10 mmol, 0.2 eq.) in 5 mL of oDCB was added dropwise through the rubber septum with a syringe. The reaction was maintained for 48 h under continuous stirring at 150 °C. The mixture was then cooled down to room temperature and filtered under vacuum on a polyamide filter (0.45 μm pore size, Sartorius Stedim). The black powder was washed thoroughly with acetone, DCM and ethanol. Finally, the powder was dried for 2 days under vacuum at 60 °C.

2.3.2. GNP oxidation

The GNP oxidation protocol was adapted from the method of

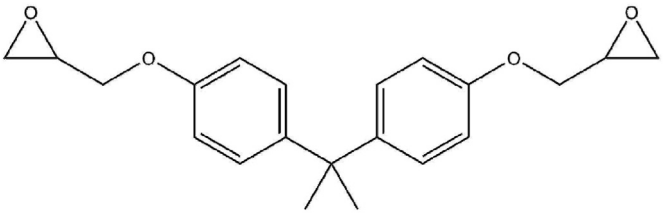

Diglycidyl ether of bisphenol A (DGEBA)

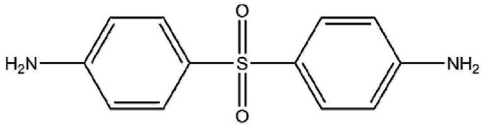

4,4'-Diaminodiphenyl sulfone (DDS)

Fig. 1. Chemical structures of epoxy resin (DGEBA) and hardener (DDS) used in this study.

Marcano et al. [28]. GNP (1 g, 1 wt eq.) was introduced in a 250 mL flask with a mixture 9:1 of concentrated H_2SO_4/H_3PO_4 (120:13.3 mL). Then, $KMnO_4$ (6 g, 6 wt eq.) was added in ~10 portions producing a slight exotherm. The mixture was heated to 50 °C and stirred for 1 h. The reaction mixture was poured onto ice (143 g) and H_2O_2 30% (5 mL) was added slowly. The product was left to settle overnight and the supernatant was decanted away. The remaining fraction was diluted with distilled water. The mixture was then centrifuged at 9000 rpm for 1 h, and the supernatant was decanted away. The remaining material was then washed in succession with 50 mL water, 50 mL HCl 10%, 50 mL water (2x) and 50 mL ethanol (2x). For each wash, the material is centrifuged at 10.000 rpm for 1 h, the supernatant decanted away and the solid material is re-dispersed using sonication (Selecta Ultrasons-HD bath, 120 W). Finally, the solid material was coagulated with 50 mL Et_2O, filtered over a PTFE filter and dried for 2 days under vacuum at room temperature.

2.4. Preparation of epoxy/(ox-, cm-)GNP nanocomposites

Pristine or chemically modified GNP (557 mg for 2 % wt.) were mixed with 20 g of DGEBA (DER 332). The mixture was heated to 130 °C and mechanically stirred or probe sonicated for 30 min. After dispersion of the fillers, 7.3 g of (solid) hardener (DDS) were added to the mixture and homogenised for 10 min with continuous stirring (or sonication). Finally, the nanocomposite mixture was poured into a silicon mould and degassed in vacuum oven for 1 h. The epoxy nanocomposite was cured at 180 °C for 2 h followed by a post-curing step at 220 °C for another 2 h. The resin-to-curing agent weight ratio was 100:36.5. The probe ultrasonicator used is a Hielscher UP400S (400 W, 24 kHz) with power and phase regulation allowed via the sonotrode H3. The phase used was 0.5 with power at 60%. Schematic of the production process can be viewed in the S.I (Fig. S1).

2.5. Characterization

Fourier transform infrared spectroscopy (FTIR) was conducted on a TENSOR 27 instrument (Bruker Optik GmbH, Ettlingen, Germany) in the attenuated total reflection (ATR) mode with a diamond crystal. The background and sample spectra were recorded at 4 cm^{-1} spectral resolution across the 4000 - 500 cm^{-1} range. ^1H and ^{13}C nuclear magnetic resonance (NMR) spectra were recorded on an AVANCE III HD Bruker spectrometer operating at a proton frequency of 600 MHz and equipped with a 5 mm BBO-probe. NMR samples were dissolved in deuterated chloroform ($CDCl_3$). The spectra were referenced relative to tetramethylsilane (TMS).

For solvent affinity tests, the pristine fillers (GNP), azidopropanol modified GNP (cm-GNP) and oxidized-GNP (ox-GNP) were dispersed in a mixture of 1:1 oDCB/distilled water. The powders (1 mg) were dispersed in a 2 mL Eppendorf, in a sonication bath, followed by homogenization with a vortex mixer at maximum speed (RS-VA 10, Phoenix instrument). Pictures were taken 15 min after dispersion to allow any remaining aggregates to sediment.

Scanning electron microscopy (SEM) micrographs were acquired on a Quanta FEG 200 (FEI) microscope. For the coverage percentage of the fillers, all images were acquired with similar parameters (HV: 15.00 kV, Mag.: 100x, P: 100 Pa, WD ~ 9–10 mm Det.: LFD). For each sample, a minimum of six different pictures were randomly taken over the composite surface. All sample were previously polished with an automated procedure on a Struers Tegramin 25. SEM micrographs were post-treated with *ImageJ* to extract the surface coverage (in %) of the fillers on a section (~1.8 mm^2) of the polymer composite.

Raman spectra were acquired for GNP powders and epoxy composites using a Raman spectroscope (Renishaw inVia micro-Raman spectrometer) with a 532 nm laser. GNP powders samples were prepared by drop casting a suspension of GNP powder in Hexane onto silicon (SiO_2/Si) wafers. The Raman spectra were measured at a magnification of 100X in a wavenumber range of 900–2000 cm^{-1} for G and D peak analyses.

X-ray photoelectron spectroscopy (XPS) analyses were carried out with a XPS Axis Ultra DLD from Kratos Analytical Ltd. hemispherical electron analyser using a monochromated Al Kα source (1486.6 eV), at a base pressure of 1×10^{-09} mbar. Charging effects were compensated with low-energy electrons (5 eV), and binding energies were calibrated using the main C 1s peak at 284.0 eV as internal standard.

Thermogravimetric analysis (TGA) was performed on a Mettler Toledo TGA 2 instrument. The samples were placed in alumina crucibles and heated under inert atmosphere (N_2 gas) from room temperature to 800 °C at a heating rate of 10 K/min.

To characterize the 3D morphological features of the composites of this study, micro-computed X-ray tomography (μCT) was employed. To this end, 4 mm × 1 mm × 1 mm rectangular samples were scanned by means of a μCT EasyTom 160 fabricated by RX solutions. The acquisition was conducted with an x-ray source voltage of 40 kV, current of 90 μA and power of 3.6 W. These parameters enabled a good phase contrast between the epoxy matrix and graphene fillers. The frame rate was set to 2 frames per second and the number of average frames was 5. During the scan, the samples were rotated 360° in angular steps of 0.25°, providing 1440 projections. The source-object-distance was set at 3.5 mm while the source-detector-distance was 255 mm, enabling a voxel size of 1.75 μm. The 3D reconstruction of the samples volume was carried out by means of the software Xact64 (RX Solutions). First, the 2D projections were treated by performing a spot correction, geometrical offset adjustment and ring artefact removal. Then, 3D reconstruction was achieved by superposing these projections through the filtered back projection algorithm included in the software.

For a better understanding of the tomographic results, the commercial software Avizo was used for image treatment and analysis. First, a sub-volume of 0.65 mm^3 was extracted from the scanned samples. Then, images were de-noised by using a median filter option [29]. This allowed replacing the grey level of each pixel by the median value of the grey levels of a certain number of neighbour pixels. A median filter of 18 neighbours was found to be the best compromise for eliminating artefacts while preserving the elements of interest. Then, heterogeneities in the material were segmented by thresholding the greyscale intensity histogram. After segmentation, objects whose dimension were below 4 μm were filtered. This allowed eliminating the uncertainty caused by the small objects beyond the resolution of our equipment. Finally, images were statistically characterized through different morphological parameters. These consisted in the equivalent diameter (D_{eq}), corresponding to the diameter of a sphere of same volume than the studied object; the volume fraction ($V_{fraction}$), which is the relative volume between the studied phase and the total studied volume, and the number of heterogeneities per unit volume (ρ_h). The definition of these expressions are:

$$D_{eq} = \sqrt[3]{\frac{6V}{\pi}}; \quad (1)$$

$$V_{fraction} = \frac{\sum_{i=1}^{n} V_i}{V_{total}}; \quad (2)$$

$$\rho_h = \frac{N_o}{V_{total}} \quad (3)$$

where N_o is the number of detected objects, V is the volume of the object and V_{total} is the total analysed volume.

The nanocomposites thermal conductivity was measured under normal temperature and pressure conditions with a Hot Disk TPS 2500S instrument according to the ISO 22007-2 standard. All samples were obtained from the same silicone mould (6 * 2.5 * 2 cm^3). The composite bar was debited in two pieces using a precision cutting machine (Struers Accutom-50). To avoid any error due to sedimentation or inhomogeneous dispersion of the fillers, each faces of the pieces ("top" and "bottom") were put in contact with the hot disk sensor (c5465, kapton coated). Hence, a minimum of four measurements were recorded (*i.e.* top-top, top-bottom, bottom-top and bottom-bottom) for all composites (See Figure S2).

3. Results and discussion

3.1. Organic syntheses

Azido-propanol (**2**) was synthesized with a simple, straightforward (one-step) and green (aqueous medium) method. The halogen from the aliphatic alkyl halide **1** was substituted with an azide (using NaN_3) in aqueous medium under refluxing conditions within a few hours with quantitative yield to form the corresponding aliphatic azide **2** (Fig. 2). The substitution of halogens by an azide group is well-established in the literature [30].

The successful synthesis was confirmed by FT-IR (Fig. 3) and NMR spectroscopy (Fig. S3 and S4). The chemical shift ~3.4 ppm in the ^{1}H NMR spectrum is characteristic of the methylene-azide protons (-C**H**$_2$-N_3) and the chemical shift ~ 50 ppm in the ^{13}C NMR spectrum is characteristic of the methylene-azide carbon (-**C**H$_2$-N_3). The azide group exhibits a very characteristic peak in FT-IR spectrum around ~2100 cm^{-1} associated to the asymmetric stretching of azide bonds [31]. The broad peak ~3300 cm^{-1} is visible before and after modification and corresponds to the O–H stretching. The doubled peak at ~2900 cm^{-1} arises from the C–H stretching of the carbonated skeleton. It is noteworthy that the strong peak at ~700 cm^{-1} associated to C–Cl stretching vanishes after substitution with the azide group, which supports the substitution of the chlorine by an azide.

3.2. GNP functionalization and characterization

The chemical modification of GNP was carried out by thermal decomposition of the as-synthesized organic azide in a suspension of the nanocarbon powder. It has been reported that azides undergo spontaneous decomposition at high temperature, or under UV irradiation, into a nitrene and nitrogen gas [32]. The reactive nitrene, nitrogen equivalent of carbene, produced *in situ* are then grafted onto the surface of the GNP forming a 3-membered aziridine ring (Fig. 4a). For comparison with a classic modification method, oxidation of the GNP was carried out following the method of Marcano et al. [28], as described in the experimental section (Fig. 4b).

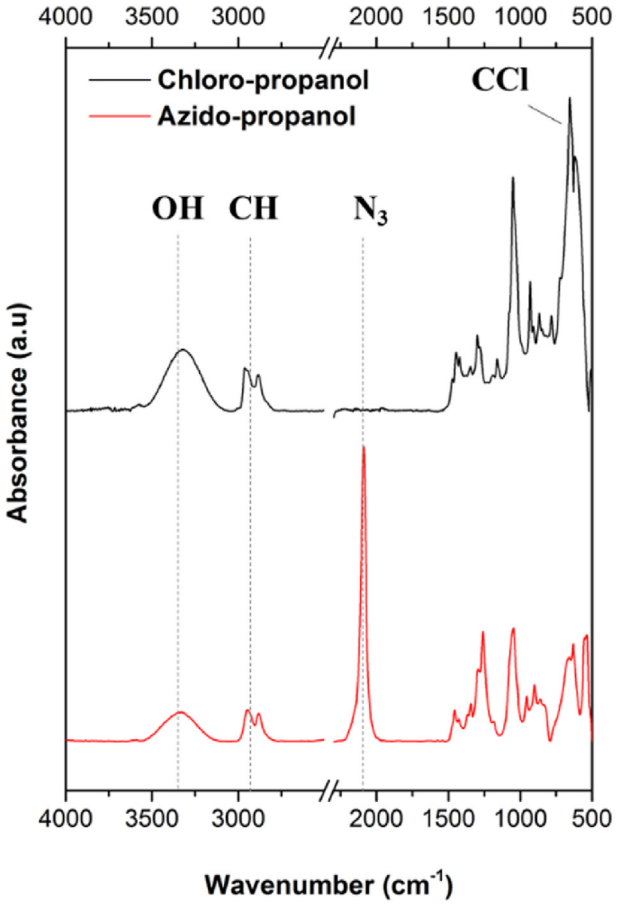

Fig. 3. FTIR spectra of the starting material chloro-propanol (black) and the synthesized azido-propanol (red). (A colour version of this figure can be viewed online.)

The mechanism for aziridine ring formation has two options (Fig. 5). The first and most commonly described in the literature is the above mentioned formation of reactive nitrene. The nitrenes are able to react with double C=C bonds considered as olefins on the surface of GNP by [2 + 1]cycloaddition to form an azirdine ring. However, it has been also mentioned that aliphatic azides might undergo a direct [3 + 2] cycloaddition followed by elimination of nitrogen gas leading to the final aziridine ring [33]. In both cases, nitrogen elimination leads to the aziridine formation. In our experiments, gaseous decomposition was indeed observed during the reaction.

The interfacial thermal resistance in nanocarbon/polymer composites comes from the mismatch of the acoustics and vibrational properties of the two different materials [34]. Therefore, the functionalization should match some of the vibrational properties of the epoxy matrix [14]. To this end, we chose an alkyl moiety, with a polar dangling unit to improve the interaction with the polar epoxy matrix. Moreover, in order to achieve an efficient thermal transfer across the GNP/epoxy interface we limited the molecular chain length in order to reduce the length of the interface and the

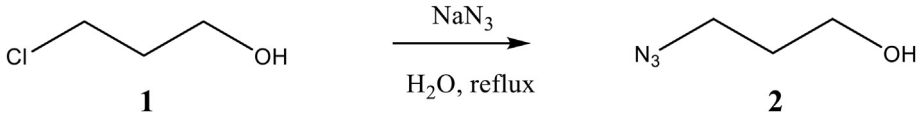

Fig. 2. Synthesis of 3-azido-1-propanol (2) from 3-chloro-1-propanol (1).

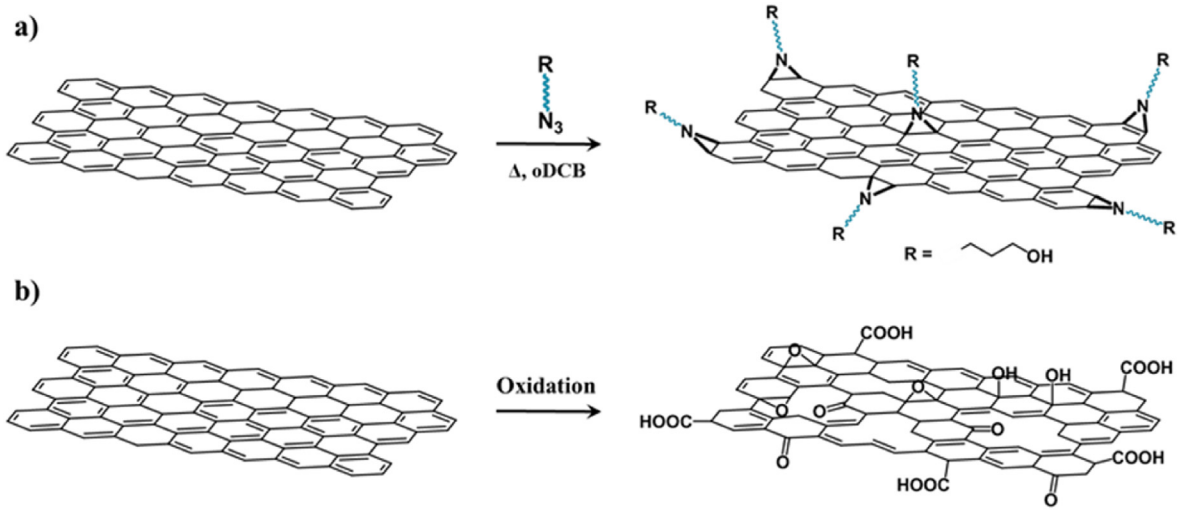

Fig. 4. GNP functionalization via a) nitrene chemistry and b) oxidation. (A colour version of this figure can be viewed online.)

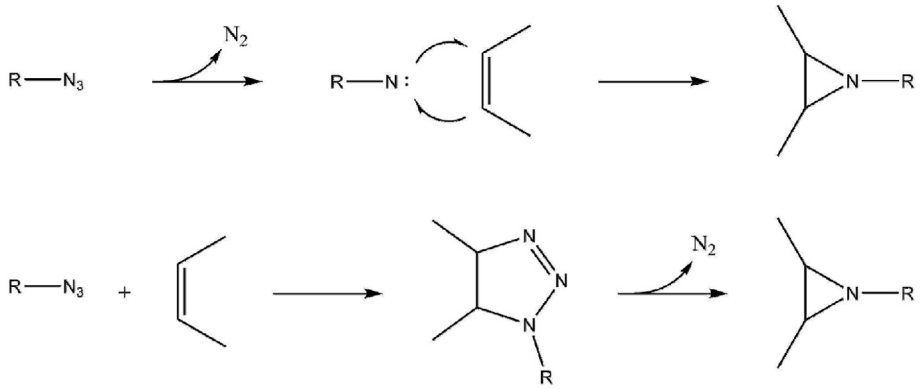

Fig. 5. Reaction pathways leading to the formation of an aziridine ring from olefins and azides. First, in-situ generation of a nitrene leading to a [2 + 1] cycloaddition with the olefin. Second, formation of a triazoline ring via a [3 + 2] cycloaddition followed by nitrogen elimination.

route travelled by the heat wave [35].

3.2.1. Solvent affinity

In contrast to pristine GNP, both functionalized GNP have better affinity for water than oDCB (Fig. 6). Pristine GNP, mainly made up of sp^2 carbon, is nonpolar and thus hydrophobic in nature.

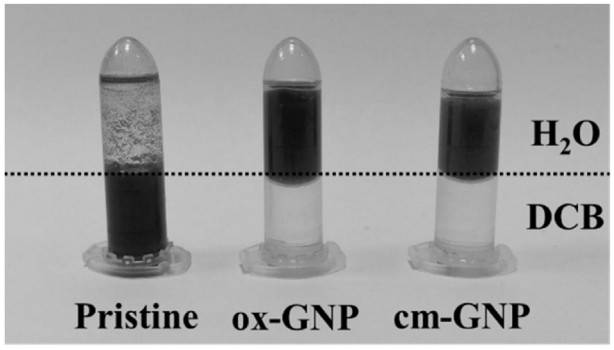

Fig. 6. Solvent affinity of the different GNP powders. Pristine GNP lies in the denser oDCB layer (bottom layer). In contrast, the chemically-modified and oxidized GNP have a better affinity for the aqueous layer (top layer).

Therefore, it lies preferably at bottom, in the organic layer. Oxidation of nanocarbons is a very common way to improve the suspension quality of nonpolar graphene in aqueous and polar media. Fig. 6 confirms the successful oxidation with a high affinity of ox-GNP for water compared to oDCB. Similarly, a small layer of propanol anchored on the GNP surface allows the cm-GNP fillers to go from the organic layer to the aqueous layer. The dispersion is stable for several days compared with the pristine GNP, which starts to sediment after few hours in oDCB.

3.2.2. Thermogravimetric analysis (TGA)

Thermogravimetric analysis provides valuable information on the functionalization yield. Indeed, mass losses, in comparison to pristine GNP, are associated with the organic surface moieties decomposition when TGA is carried out under inert atmosphere. Different temperatures were investigated for the functionalization of GNP via nitrene chemsitry. The GNP powder functionalized with azidopropanol at 150 °C (green dotted line) shows the highest weight loss (~20%) in Fig. 7. Thus, the highest amount of organic moieties anchored on the GNP surface is obtained at 150 °C. The thermal energy required for nitrene generation from organic azides is around 130 and 200 °C [32]. The reported temperatures in the literature are usually around 160–200 °C in order to ensure a good yield and to favour the formation of aziridine rings over triazolines from uncompleted reactions [36,37]. However, we show here that

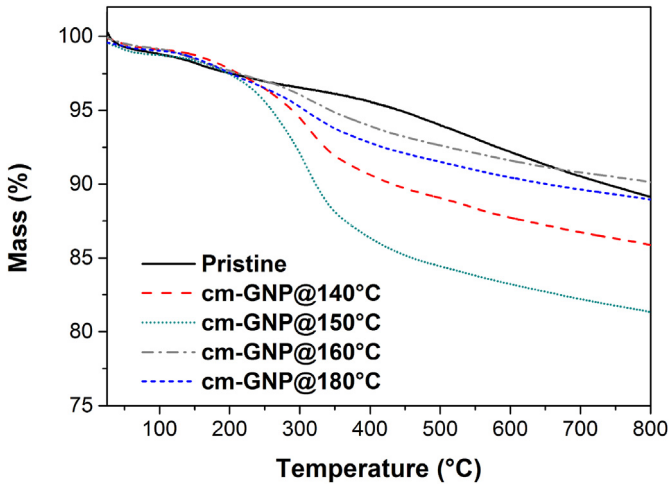

Fig. 7. Thermogravimetric analysis of GNP functionalized with azido-propanol at different reaction temperatures. (A colour version of this figure can be viewed online.)

high temperatures should no always be privileged for nitrene functionalization. The thermolysis of the azide group is triggered around 140 °C, as depicted in Fig. 7. The functionalization yield increase with increasing the temperature to 150 °C, as the azide thermolysis is facilitated by the temperature increase. However, upon further temperature increase, the thermal energy not only trigger the thermolysis of the azide but also leads to a decomposition of the molecule. This work highlights the necessity to find a right balance between enough energy to trigger the thermolysis and too-much energy leading to a decomposition of the molecule. It is noteworthy that the functionalization was also attempted in DMF, at 150 °C for different times and concentrations, but none of the attempts was found effective for functionalization (Fig S5).

Thermogravimetric analysis was also performed on the oxidized sample and is presented in Fig. 8, along with the pristine filler and cm-GNP fillers produced at 150 °C in oDCB. The weight loss observed is in good agreement with the results reported by Marcano et al. [28]. It is noteworthy that the oxidation leads to a more important modification of the graphene chemical composition with a weight loss ~50% compared to azido-propanol modified GNP with nitrene chemistry.

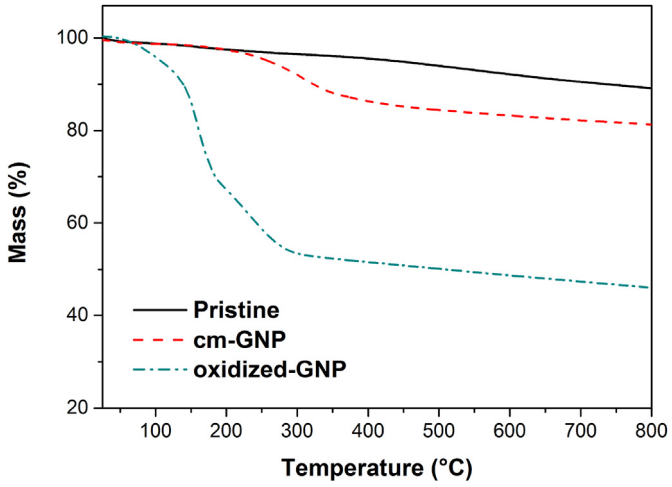

Fig. 8. Thermogravimetric analysis of Pristine GNP (black line), cm-GNP (red dashed line) and oxidized GNP (green dashed and dotted line). (A colour version of this figure can be viewed online.)

3.2.3. Raman spectroscopy

Raman spectroscopy gives information on the influence of the different functionalization methods on the carbonaceous fillers integrity. The powders were first gently dispersed in a solvent using a sonication bath for a few minutes then drop casted onto silicon wafers. The Raman spectra were acquired on different spots of the platelets (centre and edges were focussed with a confocal microscope). For comparison, a spectrum taken on the basal plane and one on the edge of GNP are presented for each sample (Fig. 9). Raman spectroscopy has been largely reported as a powerful method to characterize the defect-level in nanocarbons [38]. Graphene-related materials exhibit a main characteristic peak (G band) around ~ 1580 cm^{-1} associated to the hybridized sp^2 carbon network. Besides the G band, another characteristic peak in graphene-related materials is the D band (~1352 cm^{-1}). This peak arises from the symmetry breakdown around sp^2 carbon. In other word, structural defects (*i.e.* non sp^2-carbons, voids or C bonded to other element (H, N, O, *etc.*)) are responsible for the D band. The ratio of intensities between these two characteristic bands gives a general parameter (I_D/I_G) associated to the structural state of the nanocarbon filler. A higher ratio corresponds to a higher disorder in the microstructure.

The different ratios obtained from the Raman spectra are presented in Table 1. The pristine fillers exhibit a very low ratio, with a major contribution from the G peak. This demonstrates that the microstructure is mainly composed of undamaged sp^2 carbons. As expected, the edges of the pristine GNP exhibit a higher ratio compared to the basal plane, with more defect present at the edges. Upon functionalization with nitrene chemistry, the ratios increased similarly for both the basal plane and the edge. The nitrene chemistry allows functionalizing the basal plane, but the results demonstrate that the basal plane maintain a higher amount of crystalline domains compared to the edges. As expected, oxidized GNP shows a much higher I_D/I_G ratio, similar for the basal plane and the edge of the filler. As previously reported, oxidation damages dramatically the graphitic microstructure of the platelets [39].

This highlight the very corrosive oxidation approach that produces many oxygenated species such as carboxyl, hydroxyls, carbonyls, *etc.* Thus, oxidation comes with a profound degradation of the GNP microstructure. The nanocarbon's amorphization might have a dramatic influence on the intrinsic thermal conductivity that is directly related to the microstructure, as supported by theory [40].

3.2.4. X-ray photoelectron spectroscopy

XPS brings information on the chemical composition of the nanocarbon. The full XPS survey scans for pristine and modified-GNP gives the relative atomic concentration of the main elements (C, O, N), as presented in Table 1. Pristine GNP is mainly composed of carbon with few percent (2.9%) of oxygen. Only traces of nitrogen were recorded in the survey scan of pristine GNP. The few oxygen percent are inevitable as the edges of the GNP plates are partially oxidized. This result is in concordance with Raman spectroscopy. Upon functionalization, the relative concentration of oxygen and nitrogen increases for both oxidized-GNP and cm-GNP. The oxidized sample shows an increase from 2.9 to 35.6% oxygen, while the atomic concentration of nitrogen remains at traces level (0.9%). This confirms the successful oxidation of the platelets with a high concentration of oxygenated species on the GNP surface. The relative concentration in carbon drops down to ~60%. The cm-GNP shows an increase for both oxygen (2.9–7.4%) and nitrogen (0.2–5.3%) atomic relative percentage which corresponds for both elements to a ~5% increase. Therefore, functionalization with azido-propanol brings ~1 oxygen for 1 nitrogen which supports the structure shown in Fig. 5 where the azide moiety is thermally

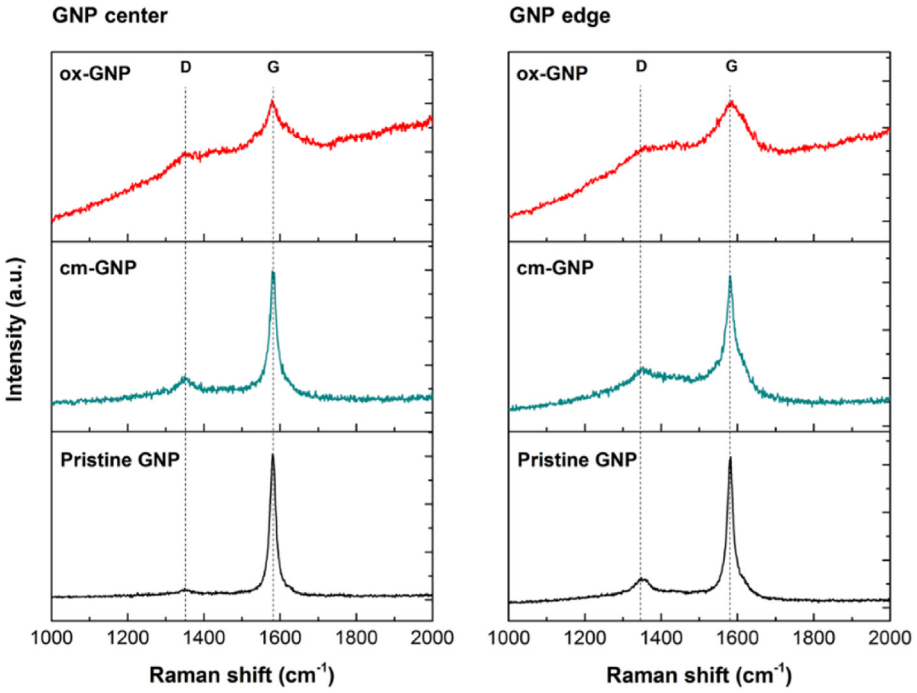

Fig. 9. –Raman spectra obtained on the center (left) or edge (right) or pristine GNP (black), cm-GNP (green) and oxidized-GNP (red). (A colour version of this figure can be viewed online.)

Table 1
Relative intensities of the G and D bands for pristine GNP, cm-GNP$_1$ and oxidized-GNP from Raman spectroscopy and associated relative elemental composition from XPS.

Sample	Raman Spectroscopy		XPS relative elemental composition (%)		
	I_D/I_G basal	I_D/I_G edge	C	N	O
Pristine GNP	0.08	0.20	96.0	0.2	2.9
cm-GNP	0.26	0.39	87.3	5.3	7.4
ox-GNP	0.79	0.79	59.3	0.9	35.6

decomposed to form an aziridine ring with only 1 nitrogen atom. Compared to the TGA results (Fig. 8), the functionalization yield appears to be lower in XPS. However, the XPS elemental composition does not distinguish the graphitic carbon (stable in TGA) from the amorphous carbon brought by the functionalization (decomposed in TGA), that may explain the difference between TGA and XPS results.

For a qualitative insight of the elemental states, the high resolution C1s XPS spectra were deconvoluted into five bands and 2 inter-band π-π* peak (Fig. 10) [41,42]. The main component observed in pristine GNP arises from the sp^2-carbons, in good agreement with the results obtained by Raman spectroscopy. In the cm-GNP spectrum, a clear band at ~286.5 eV, corresponding to C–O and/or C–N was observed, that confirms the covalent modification of GNP with –N–propanol. It is noteworthy that the major band in the C 1s XPS arises from the carbon sp^2 component, thus confirming the results obtained with Raman spectroscopy that nitrene chemistry allows maintaining a good graphitic microstructure. On the contrary, the deconvoluted C1s XPS spectrum of oxidized-GNP shows a major contribution from the band associated to C–O or C–N, which is also in good agreement with the results presented in the Raman spectrum. Two other components appear for oxidized-GNP: at ~287.9 eV associated to C=O and O–C–O species, and at 289 eV associated to O–C=O species. The C sp^2 component dramatically decreased, and the sp^3 carbon contribution increased in Fig. 10C. This is directly related to the damages induced by the oxidation on the graphitic microstructure and the reduction of the conjugated sp^2 network. This proves the successful oxidation of the support with an important amount of C–O bonds created along with a reduced sp^2 network.

The visual examination of the nanocarbons based on SEM micrographs supports the above discussion. The oxidized sample shows a wrinkled and disordered structure of the GNP compared to the thick and rigid structure of pristine GNP. The nitrene functionalized GNP is visually very similar to the pristine fillers which supports the affirmation that the fillers have maintained a graphitic microstructure with new organic molecules anchored onto the surface and preferentially on the edges.

3.3. Composite production and characterization

Epoxy nanocomposites were produced according to the procedure described in the method section. In brief, pristine or chemically modified GNP (2 wt %) were dispersed in DGEBA resin by mean of sonication or mechanical mixing. After dispersion, the hardener (DDS) was added and the mixture was stirred or sonicated for another 15 min. The nanocomposite resin was poured into a silicon mould and degassed prior to curing (Figure S6). The cured nanocomposites were debited into two pieces for thermal conductivity measurements. The two samples were polished prior to analysis in order to ensure optimized contact between the nanocomposites and the Hot Disk sensor.

3.3.1. Thermal conductivity

As expected, the nanocomposite with pristine GNP produced a high thermal conductivity (TC) enhancement compared to reference epoxy (Fig. 11). The result obtained for pristine GNP was in good agreement with previous reports with a thermal conductivity ~0.43 W/mK at 2 wt % [24,43]. It is noteworthy that pristine GNP dispersed by sonication performed better than mechanically stirred

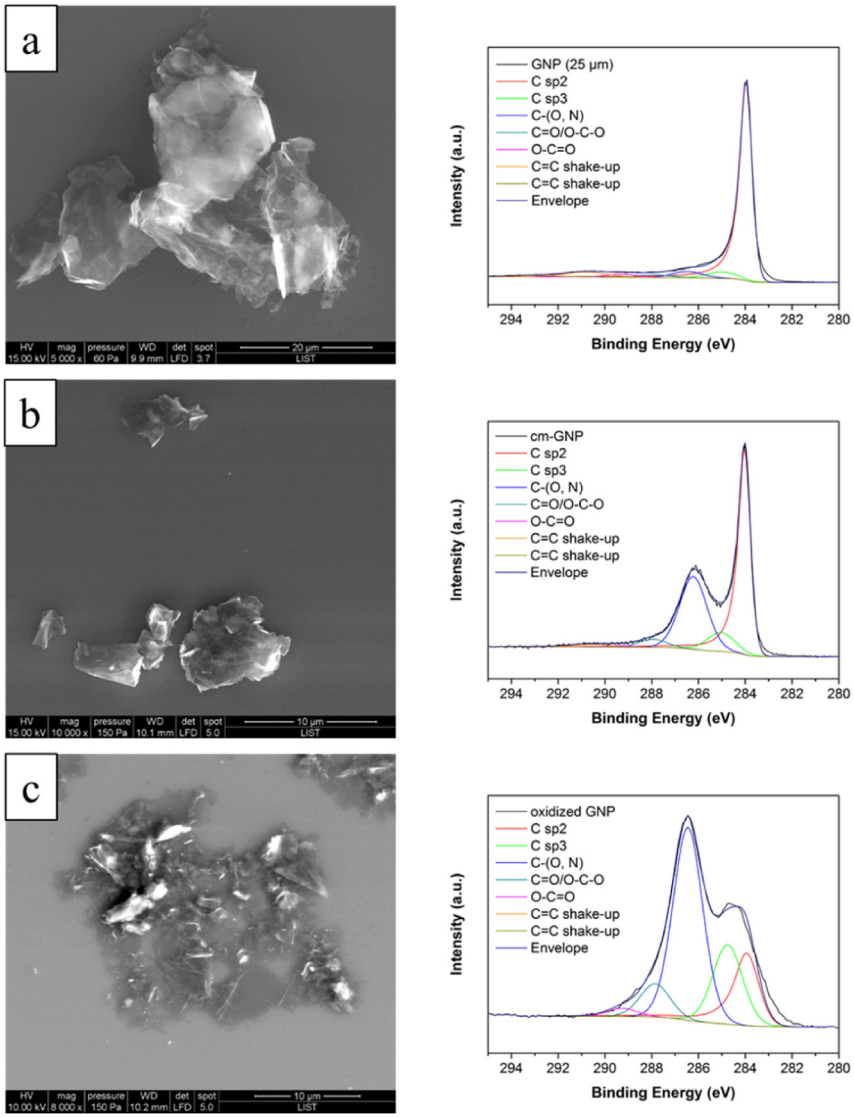

Fig. 10. SEM micrographs and C1s XPS deconvoluted spectra associated with a) pristine GNP b) cm-GNP$_1$ and c) oxidized GNP. (A colour version of this figure can be viewed online.)

pristine GNP for TC enhancement. Oxidized-GNP increased the overall thermal conductivity (~20%) compared to reference epoxy. However, the TC dropped dramatically compared to pristine GNP from 0.43 to 0.27 W/mK. The high level of disorder introduced by oxidation in the microstructure probably caused a dramatic drop of the intrinsic thermal conductivity of the fillers that reflects on the overall TC of the nanocomposite. Chemically modified GNP with nitrene chemistry, dispersed by sonication (cm-GNP sonicated), exhibited similar performances to pristine GNP. However, when the cm-GNP were mechanically dispersed, the TC increased from 0.43 (pristine GNP) to 0.49 W/mK which corresponds to a 145% increase of the thermal conductivity compared to neat epoxy resin and 30% increase compared to pristine GNP.

Thermogravimetric analysis (Fig. 12) of cm-GNP before and after ultra-sonication treatment explained the detrimental influence of ultrasounds on cm-GNP/epoxy composite TC. TGA showed a decrease in mass loss (de-functionalization) in the range 250–500 °C after sonication treatment of cm-GNP. These results were corroborated by XPS analysis of the cm-GNP before and after sonication treatment (Table S1).

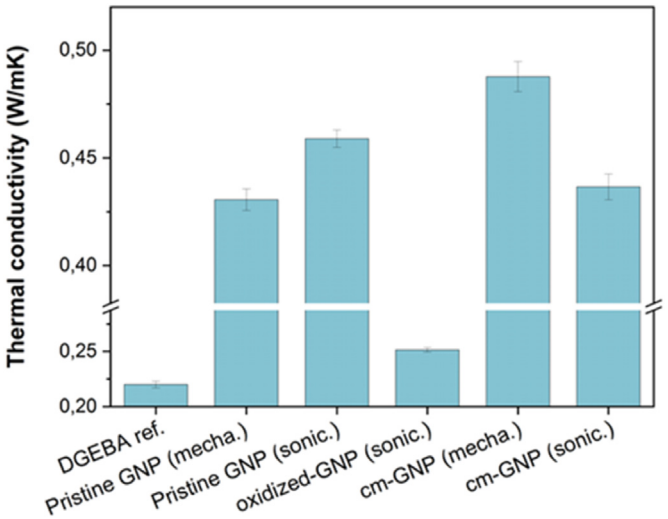

Fig. 11. Thermal conductivity of epoxy resin (DGEBA/DDS) compared to nanocomposites with pristine and chemically modified GNP. (A colour version of this figure can be viewed online.)

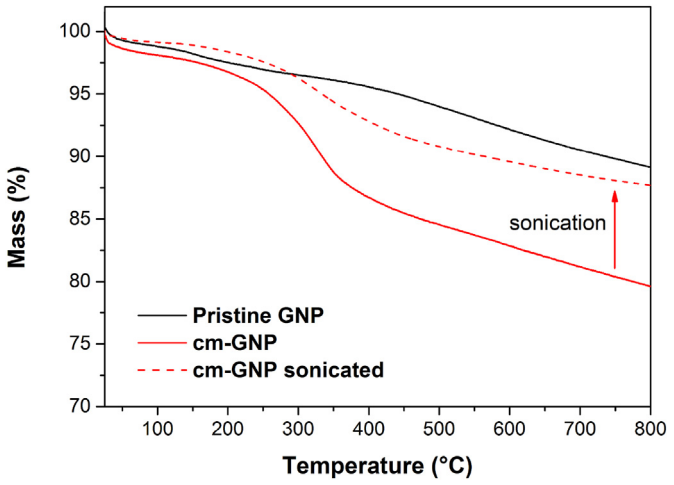

Fig. 12. Thermogravimetric analysis of chemically modified GNP with nitrene chemistry before (cm-GNP) and after (cm-GNP sonicated) a sonication treatment (30 min in DMF). (A colour version of this figure can be viewed online.)

3.3.2. SEM analysis

Post-processing of SEM micrographs with *ImageJ* allows to extract the black fillers over the greyish epoxy matrix (Fig. 13 – bottom). The ratio of the surface covered by the fillers over the total surface gives a numerical parameter, particularly helpful to compare the dispersion level in the different epoxy composites (Table 2). The SEM micrograph shows cm-GNP (Fig. 13b) more homogeneously dispersed compared to pristine GNP dispersed with the same process (*i.e.* mechanical mixing, Fig. 13a). However, the dispersion of pristine GNP with sonication is very similar to cm-GNP dispersed with the same protocol. Based on these observations, we can assume that addition of propanol molecules via nitrene chemistry promotes a more homogeneous dispersion of GNP compared to pristine GNP with mechanical mixing but sonication remains best for achieving the more homogeneous dispersion.

From a thermal conductivity point of view, two main conclusions can be drawn. First, the more homogeneously dispersed cm-GNP (Fig. 13b) increase the TC of the nanocomposites compared to pristine GNP dispersed with mechanical mixing (Fig. 13a). Second, the less homogeneous dispersion of cm-GNP (with mechanical mixing, Fig. 13b), compared to pristine GNP dispersed with sonication (Fig. 13c), still produces a higher increase of the nanocomposite TC. Thus, we can assume that functionalization plays a dual role. On one hand, it promotes and facilitates the fillers dispersion in the polymer matrix. On the other hand, it also promotes the thermal conductance at the GNP/polymer interface by reducing the interfacial thermal resistance.

3.3.3. Micro-computed X-ray tomography (μCT)

Micro-computed X-ray tomography allows reconstructing, in 3D, bulk parts of GNP/epoxy nanocomposites. The reconstructed volumes presented in Fig. 14 depict two distinct features; fillers and aggregated fillers in green (Fig. 14, top) and micro-voids in blue (Fig. 14, bottom) for pristine GNP mechanically dispersed (a), cm-GNP mechanically dispersed (b) pristine GNP dispersed with sonication (c) and oxidized-GNP dispersed with sonication (d). The 3D images clearly demonstrate the numerous presence of micro-voids surrounding the fillers inside the composites when pristine fillers are mechanically dispersed (Fig. 14 a – bottom). The voids are almost totally removed when sonication replaces mechanical stirring (Fig. 14c, d – bottom). Moreover, functionalization of GNP,

Table 2
Fillers dispersion evaluation based on imageJ treated SEM micrographs of Fig. 15.

Sample	Dispersion method	Dispersion values[a]
Pristine GNP	Mechanical mixing	28.6 ± 2.0%
Pristine GNP	Sonication	54.3 ± 3.1%
cm-GNP	Mechanical mixing	38.8 ± 3.6%
cm-GNP	Sonication	52.6 ± 4.0%

[a] The mean coverage percentage is calculated on a minimum of 7 different SEM micrographs, randomly taken over the surface of the GNP/epoxy composites.

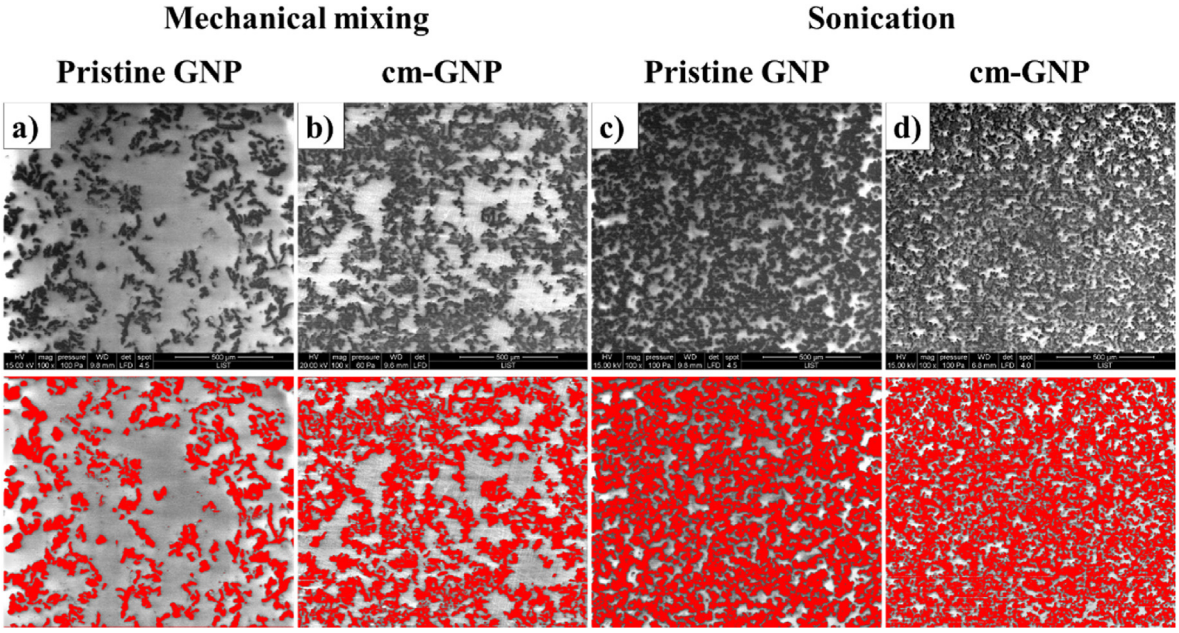

Fig. 13. SEM micrographs for epoxy nanocomposites with 2 wt % of a) pristine GNP and b) cm-GNP dispersed by mechanical mixing, c) pristine-GNP and d) cm-GNP dispersed by sonication. (A colour version of this figure can be viewed online.)

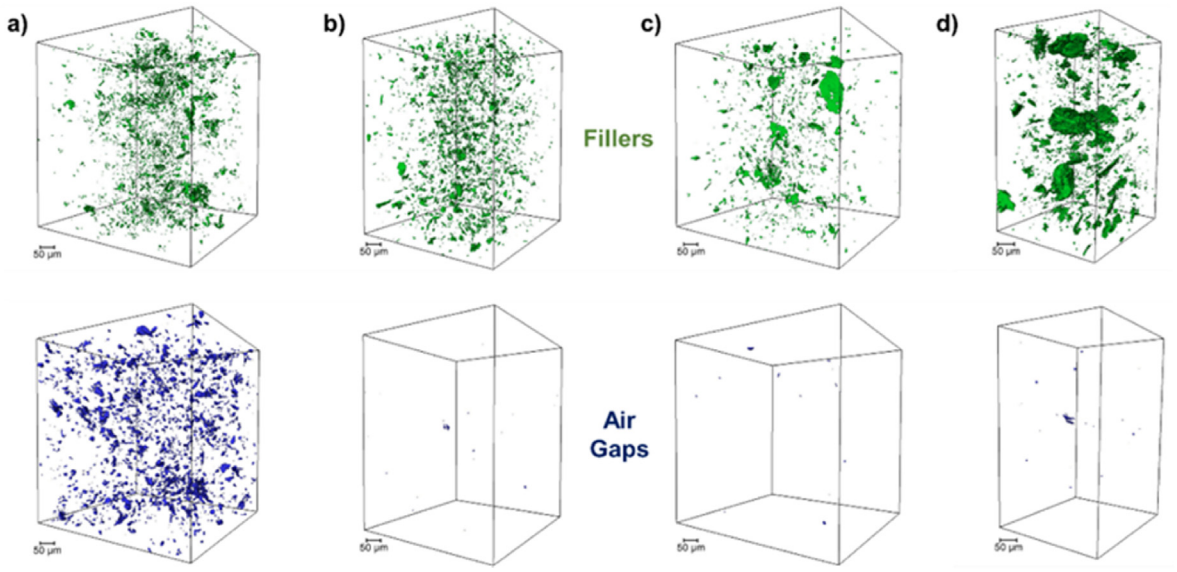

Fig. 14. Micro-computed X-ray tomography 3D reconstructions of a) pristine GNP/epoxy mechanically dispersed, b) cm-GNP/epoxy mechanically dispersed, c) pristine GNP/epoxy dispersed by sonication and d) oxidized-GNP/epoxy dispersed by sonication. Fillers are depicted in green (first row), voids in blue (second row). (A colour version of this figure can be viewed online.)

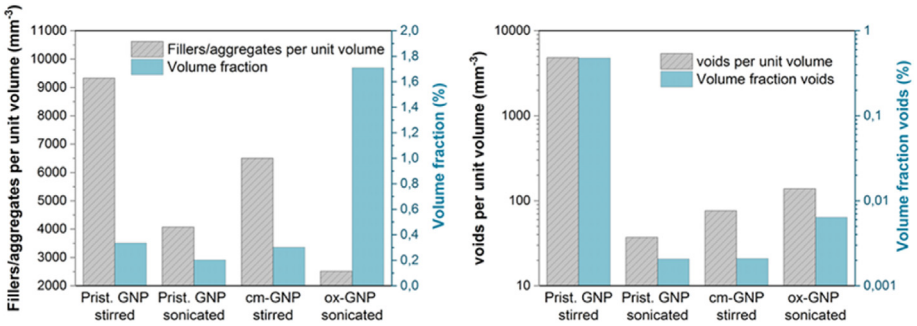

Fig. 15. Histograms of (left) the number of GNP fillers/aggregates (grey) and the associated volume fraction (green) in GNP/epoxy composites and (right) the number of voids (grey) and the associated volume fraction (green) in GNP/epoxy composites. (A colour version of this figure can be viewed online.)

similarly to sonication, helps removing the micro-voids surrounding the fillers while maintaining a mechanical mixing process (Fig. 14 b – bottom). This, of course, corroborate our above discussion, but also highlight the benefit of nanocarbon functionalization for applications where sonication cannot be used (thermoplastic engineering, extrusion, *etc.*).

The software allows counting the number of fillers (and aggregates) in the reconstructed composite volume (Fig. 15, left). The volume fraction is lower than expected because many nanocarbon structures are undetectable by μCT because they are beyond the device resolution. Moreover, the artefact correction imposed to the software deliberately suppressed small features (<4 μm) from the analysis. Sonication applied to pristine GNP produced the lowest (countable) amount of aggregates and the corresponding lowest volume of aggregates. On the opposite, mechanical dispersion of pristine GNP increases the number of aggregates and the corresponding volume. Thus, similarly to SEM analysis, μCT demonstrates the benefit of sonication for improving the dispersion state of pristine fillers. Chemical modification of GNP surface with nitrene chemistry clearly reduced the number of aggregates compared to pristine GNP dispersed with the same process. Conversely, oxidation produced less but much bigger (volume) aggregates in the final composite. This result also highlight the benefit of nitrene chemistry compared to a classic oxidation for the dispersion in a polymer composite.

Thus, μCT not only helped to obtain a 3D visualization of the bulk parts of GNP/epoxy composites and supported the SEM analyses, but also highlighted new features (micro-voids) that are invisible with conventional methods. μCT clearly demonstrated that functionalization, similarly to sonication, vanishes the micro-voids surrounding the fillers in the epoxy matrix. Therefore, we must now consider the role played by air gaps around the fillers on the thermal conductivity and the interfacial thermal resistance. To the best of our knowledge, this insulation layer surrounding the fillers has never been taken into account in the different theoretical works currently proposed in the literature. Therefore, this work might open the gate to a new model in the field of thermal conductivity in nanocarbon/polymer composites and leads to a better understanding of thermal transport in polymer composites.

4. Conclusion

A nitrene precursor, azido-propanol, was synthesized by a simple and straightforward method in aqueous solution. GNP functionalization was then achieved via thermal decomposition of the as-synthesized nitrene precursor. The successful covalent

grafting was confirmed by TGA and XPS analyses. The solvent affinity tests showed the strong influence of the grafted molecule on the chemical affinity of cm-GNP, similar to a conventional oxidation. However, Raman spectroscopy highlighted the very limited modification of the graphitic microstructure when using nitrene chemistry compared to oxidation. This non-disruptive functionalization was then observed macroscopically by thermal conductivity analysis of GNP/epoxy composites. The highly-disordered oxidized GNP led to a lower enhancement of the thermal conductivity compared to pristine GNP. By contrast, cm-GNP functionalized by nitrene produced the best results for thermal conductivity enhancement. SEM micrographs demonstrated that functionalization not only helped improving the dispersion but also improved the interaction and decreased the thermal interfacial resistance, as suggested by theory. Moreover, μCT allowed us to spot new features that were not visible by conventional analysis techniques. Indeed, μCT highlighted the presence of numerous micro-voids surrounding pristine GNP dispersed mechanically in epoxy composites. Functionalization, as well as sonication, can remove this insulating layer in epoxy composites. We believe that this new vision of GNP/polymer composites thanks to μCT could lead to a better understanding of thermal transport in GNP/polymer composites and could pave the way towards the design of new enhanced models.

CRediT authorship contribution statement

Sebastien Depaifve: Conceptualization, Methodology, Writing - original draft. **Carlos Eloy Federico:** Investigation. **David Ruch:** Project administration. **Sophie Hermans:** Supervision, Writing - review & editing. **Abdelghani Laachachi:** Conceptualization, Supervision, Funding acquisition, Writing - review & editing.

Declaration of competing interest

The authors declare that they have no known competing financial interests or personal relationships that could have appeared to influence the work reported in this paper.

Acknowledgements

This work was supported by the Luxembourg National Research Fund (AFR PhD Grant 11292782). The authors want to thank Régis Vaudemont (LIST) and Benoît Marcolini (LIST) for TGA measurements, Jean-Luc Biagi (LIST) for SEM analyses, Jérôme Guillot and Christèle Vergne (LIST) for their precious help in characterizing and interpreting XPS spectra of graphene powders.

Appendix A. Supplementary data

Supplementary data to this article can be found online at https://doi.org/10.1016/j.carbon.2020.06.035.

References

[1] M.M. Waldrop, More than moore, Nature 530 (2016) 144–147, https://doi.org/10.1038/530144a.
[2] A.A. Balandin, Thermal properties of graphene and nanostructured carbon materials, Nat. Mater. 10 (2011) 569–581, https://doi.org/10.1038/nmat3064.
[3] R. Prasher, Thermal interface materials: historical perspective, status, and future directions, Proc. IEEE 94 (2006) 1571–1586, https://doi.org/10.1109/JPROC.2006.879796.
[4] N. Burger, A. Laachachi, B. Mortazavi, M. Ferriol, M. Lutz, V. Toniazzo, D. Ruch, Alignments and network of graphite fillers to improve thermal conductivity of epoxy-based composites, Int. J. Heat Mass Tran. 89 (2015) 505–513, https://doi.org/10.1016/j.ijheatmasstransfer.2015.05.065.
[5] C. Huang, X. Qian, R. Yang, Thermal conductivity of polymers and polymer nanocomposites, Mater. Sci. Eng. R Rep. 132 (2018) 1–22, https://doi.org/10.1016/j.mser.2018.06.002.
[6] P. Greil, Perspectives of nano-carbon based engineering materials, Adv. Eng. Mater. 17 (2015) 124–137, https://doi.org/10.1002/adem.201400110.
[7] A.A. Balandin, S. Ghosh, W. Bao, I. Calizo, D. Teweldebrhan, F. Miao, C.N. Lau, Superior thermal conductivity of single-layer graphene, Nano Lett. 8 (2008) 902–907, https://doi.org/10.1021/nl0731872.
[8] N. Burger, A. Laachachi, M. Ferriol, M. Lutz, V. Toniazzo, D. Ruch, Review of thermal conductivity in composites: mechanisms, parameters and theory, Prog. Polym. Sci. 61 (2016) 1–28, https://doi.org/10.1016/j.progpolymsci.2016.05.001.
[9] L. Hu, T. Desai, P. Keblinski, Determination of interfacial thermal resistance at the nanoscale, Phys. Rev. B Condens. Matter 83 (2011), https://doi.org/10.1103/PhysRevB.83.195423.
[10] L.C. Tang, Y.J. Wan, D. Yan, Y.B. Pei, L. Zhao, Y.B. Li, L. Bin Wu, J.X. Jiang, G.Q. Lai, The effect of graphene dispersion on the mechanical properties of graphene/epoxy composites, Carbon N. Y. 60 (2013) 16–27, https://doi.org/10.1016/j.carbon.2013.03.050.
[11] S.A. Shojaee, A. Zandiatashbar, N. Koratkar, D.A. Lucca, Raman spectroscopic imaging of graphene dispersion in polymer composites, Carbon N. Y. 62 (2013) 510–513, https://doi.org/10.1016/j.carbon.2013.05.068.
[12] Z. Xu, M.J. Buehler, Nanoengineering heat transfer performance at carbon nanotube interfaces, ACS Nano 3 (2009) 2767–2775, https://doi.org/10.1021/nn9006237.
[13] M. Wang, D. Galpaya, Z.B. Lai, Y. Xu, C. Yan, Surface functionalization on the thermal conductivity of graphene–polymer nanocomposites, Int. J. Smart Nano Mater. 5 (2014) 123–132, https://doi.org/10.1080/19475411.2014.904828.
[14] Y. Wang, H.F. Zhan, Y. Xiang, C. Yang, C.M. Wang, Y.Y. Zhang, Effect of covalent functionalization on thermal transport across graphene–polymer interfaces, J. Phys. Chem. C 119 (2015) 12731–12738, https://doi.org/10.1021/acs.jpcc.5b02920.
[15] S. Lin, M.J. Buehler, The effect of non-covalent functionalization on the thermal conductance of graphene/organic interfaces, Nanotechnology 24 (2013), https://doi.org/10.1088/0957-4484/24/16/165702.
[16] Z. Sekhavat Pour, M. Ghaemy, Polymer grafted graphene oxide: for improved dispersion in epoxy resin and enhancement of mechanical properties of nanocomposite, Compos. Sci. Technol. 136 (2016) 145–157, https://doi.org/10.1016/j.compscitech.2016.10.014.
[17] W. Li, X.Z. Tang, H. Bin Zhang, Z.G. Jiang, Z.Z. Yu, X.S. Du, Y.W. Mai, Simultaneous surface functionalization and reduction of graphene oxide with octadecylamine for electrically conductive polystyrene composites, Carbon N. Y. 49 (2011) 4724–4730, https://doi.org/10.1016/j.carbon.2011.06.077.
[18] C. Vallés, I.A. Kinloch, R.J. Young, N.R. Wilson, J.P. Rourke, Graphene oxide and base-washed graphene oxide as reinforcements in PMMA nanocomposites, Compos. Sci. Technol. 88 (2013) 158–164, https://doi.org/10.1016/j.compscitech.2013.08.030.
[19] Z. Zhang, H.C. Schniepp, D.H. Adamson, Characterization of graphene oxide: variations in reported approaches, Carbon N. Y. 154 (2019) 510–521, https://doi.org/10.1016/j.carbon.2019.07.103.
[20] S. Lin, M.J. Buehler, Thermal transport in monolayer graphene oxide: atomistic insights into phonon engineering through surface chemistry, Carbon N. Y. 77 (2014) 351–359, https://doi.org/10.1016/j.carbon.2014.05.038.
[21] X. Shen, X. Lin, J. Jia, Z. Wang, Z. Li, J.K. Kim, Tunable thermal conductivities of graphene oxide by functionalization and tensile loading, Carbon N. Y. 80 (2014) 235–245, https://doi.org/10.1016/j.carbon.2014.08.062.
[22] H. Zhang, A.F. Fonseca, K. Cho, Tailoring thermal transport property of graphene through oxygen functionalization, J. Phys. Chem. C 118 (2014) 1436–1442, https://doi.org/10.1021/jp4096369.
[23] C.C. Teng, C.C.M. Ma, C.H. Lu, S.Y. Yang, S.H. Lee, M.C. Hsiao, M.Y. Yen, K.C. Chiou, T.M. Lee, Thermal conductivity and structure of non-covalent functionalized graphene/epoxy composites, Carbon N. Y. 49 (2011) 5107–5116, https://doi.org/10.1016/j.carbon.2011.06.095.
[24] S.H. Song, K.H. Park, B.H. Kim, Y.W. Choi, G.H. Jun, D.J. Lee, B.-S. Kong, K.-W. Paik, S. Jeon, Enhanced thermal conductivity of epoxy-graphene composites by using non-oxidized graphene flakes with non-covalent functionalization, Adv. Mater. 25 (2013) 732–737, https://doi.org/10.1002/adma.201202736.
[25] T. Luo, J.R. Lloyd, Enhancement of thermal energy transport across graphene/graphite and polymer interfaces: a molecular dynamics study, Adv. Funct. Mater. 22 (2012) 2495–2502, https://doi.org/10.1002/adfm.201103048.
[26] M.D. Losego, M.E. Grady, N.R. Sottos, D.G. Cahill, P.V. Braun, Effects of chemical bonding on heat transport across interfaces, Nat. Mater. 11 (2012) 502–506, https://doi.org/10.1038/nmat3303.
[27] K. Suggs, D. Reuven, X.-Q. Wang, Electronic properties of cycloaddition-functionalized graphene, J. Phys. Chem. C 115 (2011) 3313–3317, https://doi.org/10.1021/jp111637b.
[28] D.C. Marcano, D.V. Kosynkin, J.M. Berlin, A. Sinitskii, Z. Sun, A. Slesarev, L.B. Alemany, W. Lu, J.M. Tour, Improved synthesis of graphene oxide, ACS Nano 4 (2010) 4806–4814, https://doi.org/10.1021/nn1006368.
[29] K. Schörne, Development of Methods for Scatter Artifact Correction in Industrial X-Ray Cone-Beam Computed Tomography, Technical University of Munich, 2012.
[30] E.F.V. Scriven, K. Turnbull, Azides: their preparation and synthetic uses, Chem. Rev. 88 (1988) 297–368, https://doi.org/10.1021/cr00084a001.
[31] E. Lieber, C.N.R. Rao, T.S. Chao, C.W.W. Hoffman, Infrared spectra of organic azides, Anal. Chem. 29 (1957) 916–918, https://doi.org/10.1021/

ac60126a016.
[32] H. Dürr, H. Kober, Triplet states from azides, Top. Curr. Chem. (1976) 89–114, https://doi.org/10.1007/bfb0047765.
[33] M. Holzinger, J. Abraham, P. Whelan, R. Graupner, L. Ley, F. Hennrich, M. Kappes, A. Hirsch, Functionalization of single-walled carbon nanotubes with (R-)oxycarbonyl nitrenes, J. Am. Chem. Soc. 125 (2003) 8566–8580, https://doi.org/10.1021/ja029931w.
[34] E.T. Swartz, R.O. Pohl, Thermal boundary resistance, Rev. Mod. Phys. 61 (1989) 605–668, https://doi.org/10.1103/RevModPhys.61.605.
[35] A.H. Aref, H. Erfan-Niya, A.A. Entezami, Effect of alkyl functionalization on thermal conductivity of graphene oxide nanosheets: a molecular dynamics study, J. Mater. Sci. 51 (2016) 6824–6835, https://doi.org/10.1007/s10853-016-9970-z.
[36] T.A. Strom, E.P. Dillon, C.E. Hamilton, A.R. Barron, Nitrene addition to exfoliated graphene: a one-step route to highly functionalized graphene, Chem. Commun. 46 (2010) 4097–4099, https://doi.org/10.1039/c001488e.
[37] L. Lascialfari, S. Fedeli, S. Cicchi, Heterocyclic chemistry: a complete toolbox for nanostructured carbon materials, in: Prog. Heterocycl. Chem, Elsevier Ltd, 2014, pp. 29–54, https://doi.org/10.1016/B978-0-08-100017-5.00002-9.
[38] A.C. Ferrari, Raman spectroscopy of graphene and graphite: disorder, electron-phonon coupling, doping and nonadiabatic effects, Solid State Commun. 143 (2007) 47–57, https://doi.org/10.1016/j.ssc.2007.03.052.
[39] N. Morimoto, T. Kubo, Y. Nishina, Tailoring the oxygen content of graphite and reduced graphene oxide for specific applications, Sci. Rep. 6 (2016), https://doi.org/10.1038/srep21715.
[40] X. Mu, X. Wu, T. Zhang, D.B. Go, T. Luo, Thermal transport in graphene oxide - from ballistic extreme to amorphous limit, Sci. Rep. 4 (2014), https://doi.org/10.1038/srep03909.
[41] H. Estrade-Szwarckopf, XPS photoemission in carbonaceous materials: a “defect” peak beside the graphitic asymmetric peak, Carbon N. Y. 42 (2004) 1713–1721, https://doi.org/10.1016/j.carbon.2004.03.005.
[42] M.M. Bernal, A. Di Pierro, C. Novara, F. Giorgis, B. Mortazavi, G. Saracco, A. Fina, Edge-grafted molecular junctions between graphene nanoplatelets: applied chemistry to enhance heat transfer in nanomaterials, Adv. Funct. Mater. 28 (2018) 1706954, https://doi.org/10.1002/adfm.201706954.
[43] Y. Wang, J. Yu, W. Dai, Y. Song, D. Wang, L. Zeng, N. Jiang, Enhanced thermal and electrical properties of epoxy composites reinforced with graphene nanoplatelets, Polym. Compos. 36 (2015) 556–565, https://doi.org/10.1002/pc.22972.